

Second Epoch ALMA Observations of 321 GHz Water Maser Emission in NGC 4945 and the Circinus Galaxy

YOSHIAKI HAGIWARA,¹ SHINJI HORIUCHI,² MASATOSHI IMANISHI,^{3,4} AND PHILIP G. EDWARDS⁵

¹*Natural Science Laboratory, Toyo University, 5-28-20, Hakusan, Bunkyo-ku, Tokyo 112-8606, Japan*

²*CSIRO Space and Astronomy, Canberra Deep Space Communications Complex
PO Box 1035, Tuggeranong, ACT 2901, Australia*

³*National Astronomical Observatory of Japan, National Institutes of Natural Sciences (NINS)
2-21-1 Osawa, Mitaka, Tokyo 181-8588, Japan*

⁴*Department of Astronomy, School of Science, The Graduate University for Advanced Studies, SOKENDAI
2-21-1 Osawa, Mitaka, Tokyo 181-8588 Japan*

⁵*CSIRO Space and Astronomy,
PO Box 76, Epping NSW 1710, Australia*

(Accepted October, 18 2021)

ABSTRACT

We present the results of second epoch ALMA observations of 321 GHz H₂O emission toward two nearby active galactic nuclei, NGC 4945 and the Circinus galaxy, together with Tidbinbilla 70-m monitoring of their 22 GHz H₂O masers. The two epoch ALMA observations show that the strengths of the 321 GHz emission are variable by a factor of at least a few, confirming a maser origin. In the second epoch, 321 GHz maser emission from NGC 4945 was not detected, while for the Circinus galaxy the flux density significantly increased and the velocity gradient and dispersion have been measured. With the velocity gradient spanning ~ 110 km s⁻¹, we calculate the disk radius to be ~ 28 pc, assuming disk rotation around the nucleus. We also estimate the dynamical mass within the central 28 pc to be $4.3 \times 10^8 M_{\odot}$, which is significantly larger than the larger scale dynamical mass, suggesting the velocity gradient does not trace circular motions on that scale. The overall direction of the velocity gradient and velocity range of the blueshifted features are largely consistent with those of the 22 GHz maser emission in a thin disk with smaller radii of 0.1–0.4 pc and molecular outflows within ~ 1 pc from the central engine of the galaxy, implying that the 321 GHz masers could trace part of the circumnuclear disk or the nuclear outflows.

Keywords: galaxies: active — galaxies: individual (NGC 4945) — galaxies: individual (Circinus galaxy) — galaxies: nuclei — masers — submillimeter: galaxies

1. INTRODUCTION

Luminous H₂O masers in the 6₁₆–5₂₃ transition (rest frequency, $\nu_{\text{rest}} = 22.23508$ GHz) have been detected in more than 180 galaxies¹, with most of them are detected toward obscured active galactic nuclei (AGNs) hosting a Seyfert or LINER nucleus (e.g., Braatz et al. 1994, 1996; Braatz & Gugliucci 2008; Hagiwara et al. 2002, 2003, 2018; Greenhill et al. 2003a, 2009; Henkel et al. 2005; Kondratko et al. 2006; Zhang et al. 2006; Tarchi et al.

2011). These are known as H₂O megamasers. A fraction of the megamasers are classified as “nuclear masers” as they are associated with AGN-activity in their host galaxy. These exhibit spectra indicating evidence for emission from sub-parsec-scale edge-on rotating discs surrounding a super massive black hole (SMBH) (e.g., Miyoshi et al. 1995), as revealed by Very Long Baseline Interferometry (VLBI) observations at milliarcsecond (mas) angular resolution.

H₂O maser emission occurs at (sub-)millimeter wavelengths in external galaxies: the pioneering observational study of extragalactic (sub-)millimeter masers was the discovery of H₂O maser in the 3₁₃ – 2₂₀ transition ($\nu_{\text{rest}} = 183.31009$ GHz) toward the LINER galaxy NGC 3079 (Humphreys et al. 2005), which was later fol-

Corresponding author: Yoshiaki Hagiwara
yhagiwara@toyo.jp

¹ <https://safe.nrao.edu/wiki/bin/view/Main/MegamaserCosmologyProjects>

lowed by the detection of a 183 GHz maser in the nearby AGN NGC 4945 (Humphreys et al. 2016).

Hagiwara et al. (2013) conducted a search for H₂O masers in the 10₂₉–9₃₆ transition ($\nu_{\text{rest}} = 321.226$ GHz) toward H₂O megamaser galaxies, which resulted in the first extragalactic detection of a 321 GHz H₂O maser toward the center of the Circinus galaxy, obtained with the Atacama Large Millimeter/submillimeter Array (ALMA). The detection of 321 GHz H₂O maser emission toward the center of NGC 4945 from this search was reported later (Hagiwara et al. 2016; Pesce et al. 2016).

NGC 4945 is an edge-on type 2 Seyfert galaxy hosting a Compton-thick nucleus, which is heavily obscured by foreground material (e.g., Iwasawa et al. 1993; Puccetti et al. 2014). The presence of a bright transient X-ray source was reported on the south-west arm of the galaxy (Isobe et al. 2008).

The Circinus galaxy is one of the closest Compton-thick AGN with a highly obscured type 2 Seyfert nucleus (e.g., Arévalo et al. 2014; Yang et al. 2009), exhibiting a kiloparsec-scale one-sided ionization cone at a position angle of 245° (Marconi et al. 1994), which approximately agrees with that of a nuclear outflow that is optically identified on kiloparsec scales. Recent ALMA observations of thermalized CO (J=3–2) molecular line emission at $\sim 0.3''$ angular resolution have traced the circumnuclear disk ($\sim 70 \times 30$ pc) and spiral arms within ~ 200 pc of the nucleus (Izumi et al. 2018).

Prominent 22 GHz H₂O masers in the center of the galaxies (Dos Santos & Lépine 1979; Whiteoak et al. 1986; Greenhill et al. 1997b) were studied at milliarcsec (mas) spatial resolution using VLBI. In the Circinus galaxy, these observations revealed the presence of an edge-on disk-like linear structure surrounding what is a most likely a SMBH. It is claimed that some fraction of the maser emission in the Circinus galaxy traces molecular outflows emanating within ~ 1 pc from the nucleus of the galaxy (Greenhill et al. 2003b). In NGC 4945, an edge-on linear structure extending over 0.7 pc at a position angle of 45°, closer to that of the galactic disk of the galaxy, was revealed (Greenhill et al. 1997b, 2003b).

Currently, the only other extragalactic sub-millimeter H₂O line emission detected is the 5₁₅–4₂₂ transition ($\nu_{\text{rest}} = 325.15292$ GHz) toward the ultraluminous infrared galaxy (ULIRG), Arp 220 (Cernicharo et al. 2006; Galametz et al. 2016; König et al. 2017), although thermalized molecular gas emission is favoured as the origin due to lack of intensity variability and the broad line-width of the emission. Very recently, luminous 183 GHz H₂O maser emission ($L_{\text{H}_2\text{O}} \sim 10^4 L_{\odot}$) has been detected toward the ULIRG, IRAS 19254–7245 (the ‘‘Superantennae galaxy’’) at $z=0.0617$ (Imanishi et al. 2021), pro-

viding the possibility of studying dense molecular gas around a SMBH beyond the local universe.

Similar to the 22 GHz nuclear megamasers, sub-millimeter H₂O masers can probe the nuclear kinematics of AGN or dense molecular gas structures such as a rotating disk surrounding a SMBH, which provides new insights into the nuclear region of nearby AGN.

In this paper, we present new results from second epoch observations of the 321 GHz H₂O masers in NGC 4945 and the Circinus galaxy, conducted with ALMA at higher angular resolution. The optical velocity definition is adopted throughout, and the velocities are calculated with respect to the Local Standard of Rest (LSR).

2. OBSERVATIONS AND DATA REDUCTION

2.1. ALMA Cycle 4 observations

We conducted Cycle 4 ALMA observations of H₂O masers in the 10₂₉ – 9₃₆ transition ($\nu_{\text{rest}} = 321.226$ GHz) towards NGC 4945 and the Circinus galaxy for project 2016.1.00150.S (PI: Y. Hagiwara) in November 2016 and May 2017. These band 7 spectral-line observations lasted for about 30–35 minutes (approximately 8–10 minutes on-source), with 45–47 antennas, depending on the target source. The observations were made with a single spectral window (1875 MHz bandwidth) and one polarization, divided into 7680 spectral channels, yielding spectral resolutions of 244.1 kHz or 0.228 km s^{–1} at each observed frequency and a total velocity coverage of ~ 1750 km s^{–1} in order to cover Doppler-shifted emission within ± 900 km s^{–1} of the galaxy’s systemic velocity. The spectral windows were centered near the systemic velocity. After the channel smoothing to 3840 spectral points, the resulting spectral resolution is 488.3 kHz or 0.458 km s^{–1} at the observed center frequency to match that of the 22 GHz H₂O maser observations at Tidbinbilla (see Section 2.2). The observations were made at $\sim 0.3''$ angular resolution. A summary of the observations is listed in Table 1.

Data calibration was performed using the Common Astronomy Software Applications (CASA)² (McMullin et al. 2007). Flux density and bandpass calibration were performed using J1427–4206 and phase calibration was made using J1326–5256 for the observations of NGC 4945. The flux density, bandpass, and phase calibrators were J1617–5848, J1427–4206, and J1424–6807, respectively, for the Circinus galaxy. We adopted a flux density error of 10 percent, as stated in the capabilities of Cycle 4 Band 7 observations.

² <https://casa.nrao.edu>

Imaging of the calibrated data was carried out with CASA and the NRAO Astronomical Image Processing Software (AIPS) (van Moorsel, Kemball, & Greisen 1996). After phase and amplitude calibrations, the 321 GHz continuum emission of NGC 4945 and the Circinus galaxy was subtracted from the spectral line visibilities using line-free channels prior to CLEAN deconvolution of line emission. The line emission from each galaxy was separated out from the continuum emission. Imaging was performed using CASA with Briggs weighting (robust = 0.5). The synthesized beam sizes and the beam position angles used in the CLEAN process and the resultant rms noise levels in the spectral line images are listed in Table 1.

2.2. Tidbinbilla Observations

H₂O maser spectra of the galaxies in the 6₁₆ – 5₂₃ transition ($\nu_{\text{rest}}=22.23508$ GHz) were obtained using NASA Deep Space Network 70-m antenna at Tidbinbilla, DSS-43. Observations of the masers from June 2012 to April 2014 were conducted using a K-band receiver and ATNF correlator with a 64 MHz bandwidth, 2048 spectral channels, and dual circular polarization at a spectral resolution of 31.25 kHz or 0.42 km s⁻¹ (Hagiwara et al. 2013, 2016), and observations from April 2016 to May 2017 were conducted using a new K-band receiver and SAO Spectrometer with a 1 GHz bandwidth, 32000 spectral channels, and dual circular polarization (Kuiper et al. 2019) at a spectral resolution of 31.25 kHz or 0.42 km s⁻¹. We used a velocity resolution of better than ~ 1 km s⁻¹ to avoid blending of different velocity features. We adopted a telescope sensitivity of 2.6 Jy K⁻¹ to convert antenna temperature to flux density with a conservatively estimated uncertainty in the flux density of 50%, as stated in the Tidbinbilla 70 m radio telescope guide³ or in Kuiper et al. (2019). Data reduction, including baseline calibration, averaging the two circular polarizations, and flagging bad scans when required were carried out using GBTIDL⁴.

All velocities in the final plots are then converted relative to the Local Standard of Rest using the optical definition. Rms noise levels (1σ) estimated from each spectrum were ~ 50 – 300 mJy for NGC 4945 and ~ 40 – 90 mJy for the Circinus galaxy in each 0.42 km s⁻¹ channel. A summary of the observations is given in Table 2.

3. OBSERVATIONAL RESULTS

Following the approach used for the first detections in 2012, observations of the 321 GHz H₂O masers toward the center of NGC 4945 and the Circinus galaxy were centered on the phase-tracking center of the galaxy in the velocity range of $V_{\text{LSR}} = -319.5 - 1436.5$ km s⁻¹ for NGC 4945 and $V_{\text{LSR}} = -439.9 - 1314.1$ km s⁻¹ for the Circinus galaxy, covering the total velocity range of the known 22 GHz H₂O maser emission in the galaxies (Greenhill et al. 1997b; Braatz et al. 2003; Greenhill et al. 2003a). No search was made for 321 GHz maser emission beyond these velocity on this occasion. Figure 1 (left) compares the two epoch spectra of the 321 GHz H₂O maser toward the center of NGC 4945. No maser emission is detected in the second epoch (2016 November) as the strength of the maser has decreased below the detection limit (3σ) of 38 mJy. Also, a counterpart to the highly redshifted velocity feature at $V_{\text{LSR}} = 1138.6$ km s⁻¹ in the 183 GHz H₂O maser spectrum (Humphreys et al. 2016) was not found in the second epoch spectrum. Figure 1 (right) displays multi-epoch spectra of the 22 GHz H₂O maser emission that were taken from 2014 April to 2016 December with the Tidbinbilla 70-m telescope, DSS-43, showing a definite decrease of the maser intensity from mid-2014, at least, until late 2016.

Figure 2 shows spectra of the 321 GHz H₂O maser emission toward the center of the Circinus galaxy in 2012 June and 2017 May, and Figure 3 displays four-epoch spectra of 22 GHz H₂O maser emission taken at Tidbinbilla from 2012 June to 2017 May. It should be noted that the second epoch spectrum at 321 GHz and the last epoch spectrum at 22 GHz were obtained on the same date, making it possible to precisely compare velocities of the maser features between the 22 GHz and 321 GHz maser spectra.

In the Circinus galaxy, the most prominent H₂O maser emission is detected with a peak flux density of 1.56 Jy at $V_{\text{LSR}} = 601.6$ km s⁻¹ with a signal-to-noise ratio (SNR) of >80 and a 1σ rms level of ~ 19 mJy per spectral channel (Figure 3). The line-widths of the detected Doppler-shifted features may be narrower (<0.445 km s⁻¹) than one spectral channel, and narrower than the 22 GHz H₂O maser features of ~ 0.9 km s⁻¹ reported previously (Nakai et al. 1995; Greenhill et al. 1997a; Braatz et al. 2003; McCallum et al. 2005). In the second epoch observation of the 321 GHz H₂O maser, blueshifted features spanning from $V_{\text{LSR}} = 358$ – 360 km s⁻¹ are evident with a peak at $V_{\text{LSR}} = 359.29$ km s⁻¹, Doppler-shifted ~ -74 km s⁻¹ from the systemic velocity of $V_{\text{LSR}} = 433$ km s⁻¹ (de Vaucouleurs et al. 1991; Braatz et al. 2003), with a peak flux density of 198 mJy. Blueshifted features between $V_{\text{LSR}} = 200$ and 400 km

³ https://www.atnf.csiro.au/observers/docs/tid_obs_guide/tid_obs_guide.html

⁴ <https://gbtidl.nrao.edu>. Analysis of the data obtained on ATNF Correlator was made using ASAP⁵.

s^{-1} were also found in the 22 GHz maser spectrum on the same day. The most blueshifted and redshifted velocity features peak at $V_{\text{LSR}} = 260.81 \text{ km s}^{-1}$ and $V_{\text{LSR}} = 627.25 \text{ km s}^{-1}$, respectively. The total integrated intensity estimated from the spectra of the 321 GHz H_2O features detected at $\text{SNR} > 5$ between $V_{\text{LSR}} = 200$ and 800 km s^{-1} is $11.1 \pm 1.1 \text{ Jy km s}^{-1}$.

Figure 4 (left) shows the spectrum of the 321 GHz maser emission spanning from $V_{\text{LSR}} = 180\text{--}820 \text{ km s}^{-1}$ in the Circinus galaxy. Figure 4 (right) compares the two epoch spectra at 321 GHz in the highly redshifted velocity range. Signs of marginal features were suggested at $V_{\text{LSR}} = 1069 \text{ km s}^{-1}$ and $V_{\text{LSR}} = 1138.6 \text{ km s}^{-1}$ in Hagiwara et al. (2013), however these features were not identified in the second epoch spectrum. As argued by Pesce et al. (2016), it is most likely that this portion of the band is impacted by higher atmospheric absorption resulting in a somewhat higher noise level.

Sub-millimeter 321 GHz (Band 7) continuum images of NGC 4945 and the Circinus galaxy, obtained by integrating over the full frequency range (after the removal of the maser line emission), are shown in Figure 5. The continuum map of NGC 4945 shows resolved radio structures, a bright radio source and extended components, which are consistent with the map at the same frequency at $0.54''$ angular resolution (Hagiwara et al. 2016; Pesce et al. 2016), with a peak position of $\alpha(2000): 13^{\text{h}}05^{\text{m}}27.482$, $\delta(2000): -49^{\circ}28'05''.40$. The continuum map of the Circinus galaxy shows a bright radio source in the center, accompanying extended structure tracing the spiral arms (Izumi et al. 2018), with a peak position of $\alpha(2000): 14^{\text{h}}13^{\text{m}}09.954$, $\delta(2000): -65^{\circ}20'21''.01$, which is also consistent with that measured at lower angular resolution ($0.54''$) within uncertainties of $\sim 0.01''$ (Hagiwara et al. 2013). The flux densities of the 321 GHz continuum and the 321 GHz H_2O maser emission are summarized in Table 3.

All the maser features detected in our observations remain unresolved at the angular resolution of $\sim 0.33''$, or 6.9 pc. The position of the prominent blue-shifted feature peaking at $V_{\text{LSR}} = 269.2 \text{ km s}^{-1}$ is $\alpha(\text{J2000}): 14^{\text{h}}13^{\text{m}}09^{\text{s}}952$, $\delta(\text{J2000}): -65^{\circ}20'21.013''$, and that of the strongest feature at $V_{\text{LSR}} = 600.92 \text{ km s}^{-1}$ is $\alpha(\text{J2000}): 14^{\text{h}}13^{\text{m}}09^{\text{s}}949$, $\delta(\text{J2000}): -65^{\circ}20'21.019''$. From the ALMA Cycle 4 Capabilities, the image registration accuracy is $\sim \theta/20.0$, where θ is the angular resolution. Consequently, the registration accuracy is $\sim 0.33''/20 \sim 0.0165''$ in our observations and these positions of the bulk of Doppler-shifted features between $V_{\text{LSR}} = 200$ and 800 km s^{-1} in Figure 4 are consistent within that accuracy.

Figure 6 displays the velocity-integrated line intensity (0th moment), overlaid on the 321 GHz continuum (contour map), mean velocity (first moment), and velocity dispersion (second moment) maps for the 321 GHz H_2O maser in the Circinus galaxy. From the 0th moment map, the source size of the maser emission deconvolved by the synthesized beam is calculated to be $266 \pm 7 \text{ mas} \times 158 \pm 2 \text{ mas}$, corresponding to $5.6 \text{ pc} \times 3.3 \text{ pc}$, at a position angle (PA) of $35^{\circ} \pm 1^{\circ}$.

4. DISCUSSION

Given the observed flux density variability of the maser features in the spectra, it is clear that the 321 GHz H_2O emission in NGC 4945 and the Circinus galaxy occurs through the maser amplification process. Here we briefly discuss our non-detection of the 321 GHz H_2O maser in NGC 4945 and results of the image analysis of the 321 GHz maser in the Circinus galaxy.

4.1. No Detection and Intensity Variability of 321 GHz H_2O Maser in NGC 4945

From the two-epoch observations at 321 GHz in 2012 and 2016 and five-epoch single-dish observations at 22 GHz from 2014–2016, we find that strengths of the 321 GHz and 22 GHz H_2O masers vary in an apparently correlated fashion (Figure 1). The total and peak fluxes of the 321 GHz continuum in 2016 have decreased from those in 2012 (Table 3). The detected 321 GHz continuum emission of the galaxy is dominated by dust emission and contributions from the synchrotron and free-free emissions to the observed flux density are small as they decrease rapidly at sub-millimeter wavelengths. The most dominant nuclear continuum component in the center of the galaxy on the map traces the dust lanes heated by the AGN in the obscured nucleus.

Although we have only two epochs of data, there is an apparent correlation between the strength of the masers and the 321 GHz radio continuum emission from the obscured nucleus (Table 3). This is consistent with the non-detection of 321 GHz maser emission in 2016. The 321 GHz maser emission that was detected in 2012 and higher intensity of the 22 GHz maser emission in 2014 were most likely to be enhanced by increased AGN-activity through the thick dust lane in our line of sight around that period. This supports the conclusion that the 321 GHz H_2O emission in the galaxy is a nuclear maser.

If the maser is powered by X-ray emission from an AGN (e.g., Neufeld et al. 1994), then the observed intensity variability of the 22 and 321 GHz maser could be due to the central engine (e.g., Maloney 2002). In the galaxy, there is a luminous nuclear hard X-ray source

Table 1. Summary of the ALMA observations

Galaxy	RA	DEC	D	Date	N_A	θ_b, PA	t_{on}	σ_c	σ_l
	(J2000)	(J2000)	(Mpc)			(arcsec ² , °)	(min)		
(1)	(2)	(3)	(4)	(5)	(6)	(7)	(8)	(9)	(10)
NGC 4945	13 ^h 05 ^m 27 ^s .279	-49°28′04″.44	3.7	2016-11-18	45	0.381×0.313, -56.5	33	0.6	12.6
Circinus	14 ^h 13 ^m 09 ^s .906	-65°20′20″.46	4.2	2017-05-06	47	0.330×0.206, 31.0	28	0.6	13.9

NOTE—(2)-(3) Interferometry phase center positions in R.A. and Declination; (4) Adopted distances for NGC 4945 from [Tully et al. \(2013\)](#) and for Circinus from [Freeman et al. \(1977\)](#); (5) Date of observations in YYYY-mm-dd format; (6) Number of 12-m antennas used in the ALMA observations; (7) Synthesized beam size and the beam position angle; (8) On-source time for the target source; (9) Rms noise values in mJy beam⁻¹ in the clean continuum images; (10) Rms noise levels in mJy beam⁻¹ in a 488.3 kHz (0.458 km s⁻¹) spectral channel in the clean line images.

Table 2. Summary of the Tidbinbilla Observations

Galaxy	Date of Observation	ΔV	$\Delta\nu$	T_{sys}	t_{on}	σ_l
		(km s ⁻¹)	(km s ⁻¹)	(K)	(min)	(mJy)
(1)	(2)	(3)	(4)	(5)	(6)	(7)
NGC 4945	2014-04-07 ^a , 2016-04-13, 2016-10-24 2016-11-26, 2016-12-10	-250–1450	0.42	45–90	6–28	50–300
Circinus Galaxy	2012-06-26, 2012-09-07 ^b , 2016-10-24 2017-05-06	0–800	0.42	50–65	2–11	40–90

NOTE—(2) Date of observations in YYYY-mm-dd format (*a*: From published data in [Hagiwara et al. \(2016\)](#), *b*: from [Hagiwara et al. \(2013\)](#)); (3) Velocity range of 22 GHz maser spectra in Figures 1, 3; (4) Velocity resolution in each spectrum; (5) Typical values of system noise temperature; (6) Approximate on-source time for the target source; (7) Rms noise levels in the 0.42 km s⁻¹ spectral channel in each spectrum. Note that the rms values have an uncertainty due to less accurate flux density estimation (see Section 2.2). The ATNF Correlator was used for the observations up to 2014 April 7, and the Smithsonian Astrophysical Observatory (SAO) spectrometer was used for the subsequent observations.

Table 3. Measured properties of 321 GHz H₂O Maser and Continuum Emission toward Circinus galaxy and NGC 4945

Galaxy	Epoch ^a	Date ^b	Maser Line			Continuum ^d	
			Total Flux	Peak Flux	Peak Velocity ^c	Total Flux	Peak Flux
			(Jy)	(Jy beam ⁻¹)	(km s ⁻¹)	(mJy)	(mJy beam ⁻¹)
Circinus galaxy	1	2012-06-03	0.35±0.04	0.13±0.01	531.1 km s ⁻¹	55±6	40.6±4.1
	2	2017-05-06	4.3±0.4	1.56±0.16	601.6 km s ⁻¹	90.4±9.0	42.5±4.3
NGC 4945	1	2012-06-03	0.052±0.005	0.040±0.004	722.6 km s ⁻¹	543±54	136.5±13.7
	2	2016-11-18	-	-	-	475±48	61.6±6.2

NOTE—*a*: Epoch number; *b*: Date of observations in YYYY-mm-dd format; *c*: Center velocities of a maser feature in optical LSR definition; *d*: 321 GHz continuum emission from the nuclei of the galaxies

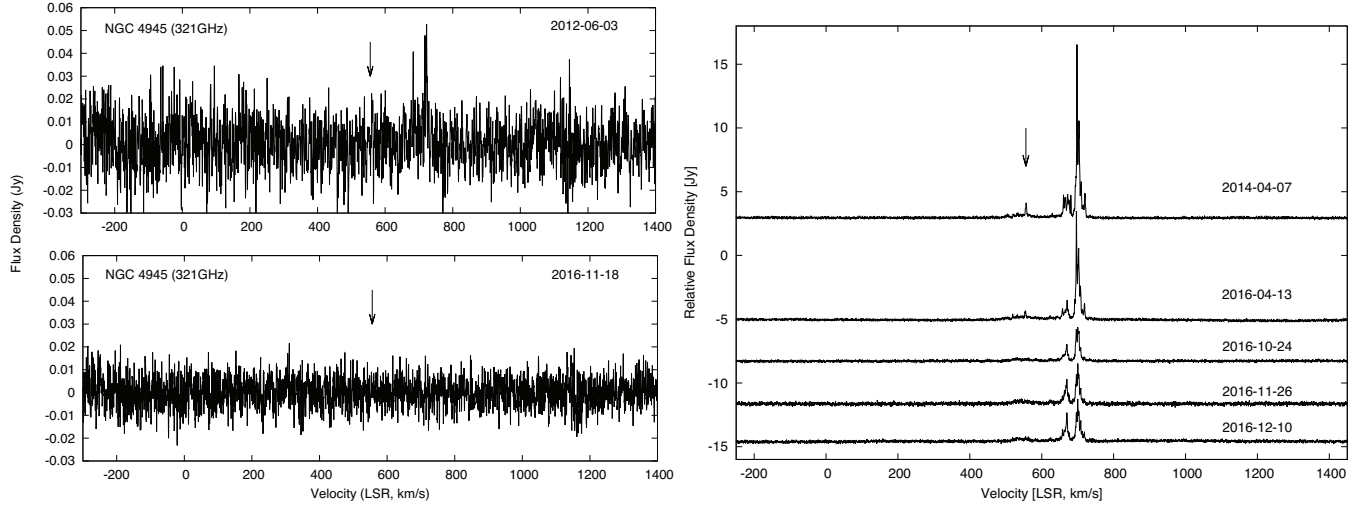


Figure 1. Spectra of H_2O maser emission toward the nucleus of NGC 4945. The LSR systemic velocity of NGC 4945, 556 km s^{-1} is denoted by the vertical arrow. *Left:* Spectra of 321 GHz H_2O maser for two epochs, obtained with ALMA. The velocity resolution is 0.458 km s^{-1} . *Right:* Spectra of 22 GHz H_2O maser, obtained with the NASA Deep Space Network 70 m antenna at Tidbinbilla, DSS-43, for five epochs from 2014 April to 2016 December. The vertical axis shows relative flux density in Jy. The amplitude scale of each 22 GHz spectrum is displayed with offsets for display purposes. The velocity resolution is 0.42 km s^{-1} . The 1σ noise levels are $\sim 28\text{--}55 \text{ mJy}$ in a 0.42 km s^{-1} channel.

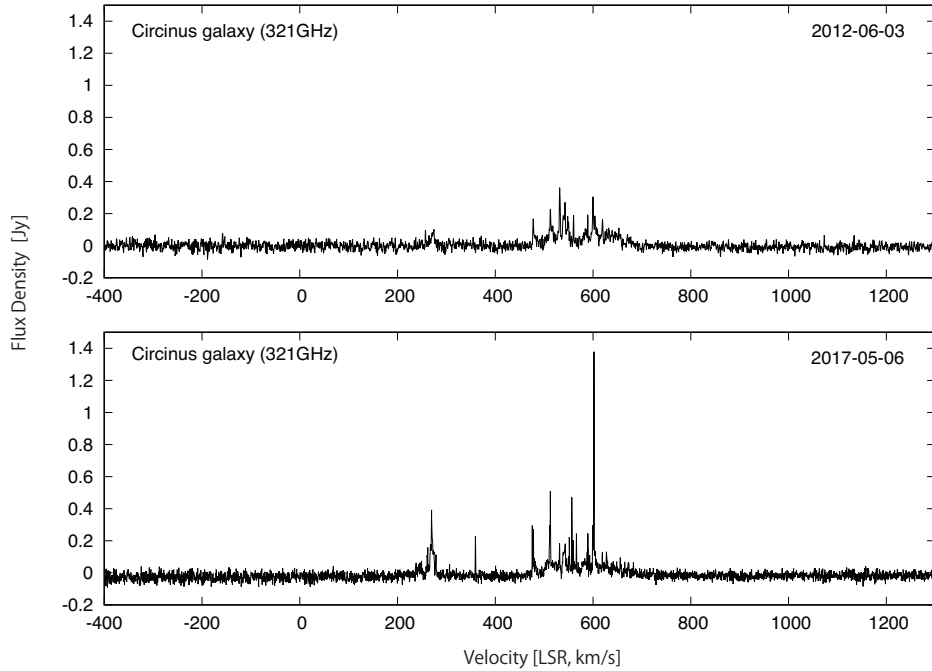


Figure 2. Comparison of 321 GHz H_2O maser spectra between 2012 June and 2017 May, obtained with ALMA. The velocity resolution is 0.458 km s^{-1} .

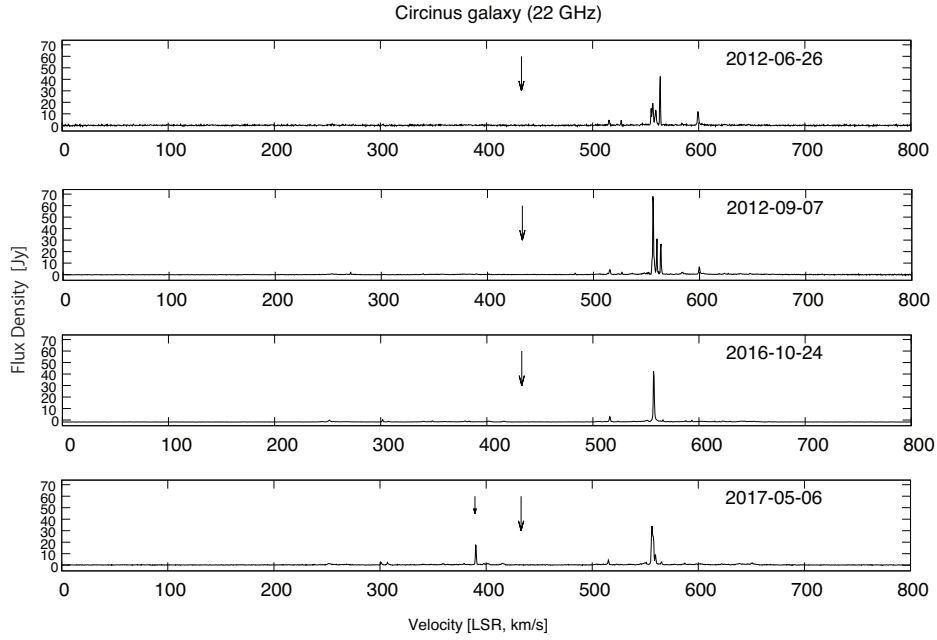


Figure 3. Spectra of 22 GHz H₂O maser for four epochs, obtained at Tidbinbilla from 2012 June to 2017 May. The LSR systemic velocity of the galaxy, 433 km s⁻¹ is indicated by a longer arrow in each epoch and a shorter arrow indicates blueshifted features centered at $V_{\text{LSR}} = 389.5$ km s⁻¹.

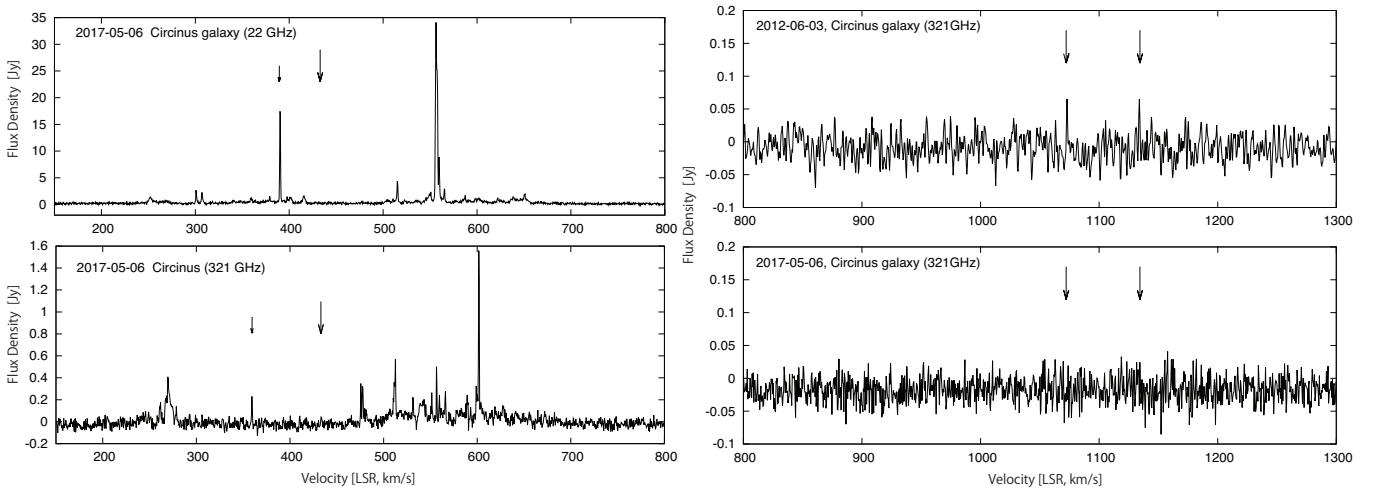


Figure 4. *Left:* Comparison of 22 GHz (*upper*) and 321 GHz (*lower*) H₂O maser spectra toward the nucleus of Circinus galaxy zoomed in the velocity range of $V_{\text{LSR}} = 150\text{--}800$ km s⁻¹ in Figure 2. Note that the both spectra were taken on 2017 May 6. The longer arrow in each panel shows the systemic velocity, and $V_{\text{LSR}} = 389.49$ km s⁻¹ (*upper*) and $V_{\text{LSR}} = 359.29$ km s⁻¹ (*lower*) features are marked by a shorter arrow. *Right:* Highly Doppler-shifted (high-velocity) 321 GHz maser spectra toward the nucleus of the Circinus galaxy in the velocity range of $V_{\text{LSR}} = 800\text{--}1300$ km s⁻¹ at epoch 1 (*upper*) and epoch 2 (*lower*). The channel spacing is 0.458 km s⁻¹. In the epoch 1 spectrum, high-velocity tentative features were suggested at $V_{\text{LSR}} = 1069$ km s⁻¹ and 1129 km s⁻¹ (shown by arrows)(Hagiwara et al. 2013). However, in the epoch 2 spectrum no emission was observed at these frequencies.

(X-ray luminosity: $L_X \sim 4 \times 10^{43}$ erg s⁻¹) buried in the Compton-thick nucleus (e.g., Marinucci et al. 2017). The X-ray luminosity is highly variable with a time scale of ~ 1 day, suggesting that the size scale of X-ray emitting region is no more than ~ 0.001 pc (Madejski et al. 2000), however it is uncertain whether this compact X-

ray region is responsible for the decreased maser intensities over the four years. Moreover, little is known about the variability of the 321 GHz masers.

4.2. The 321 GHz Maser in Circinus galaxy

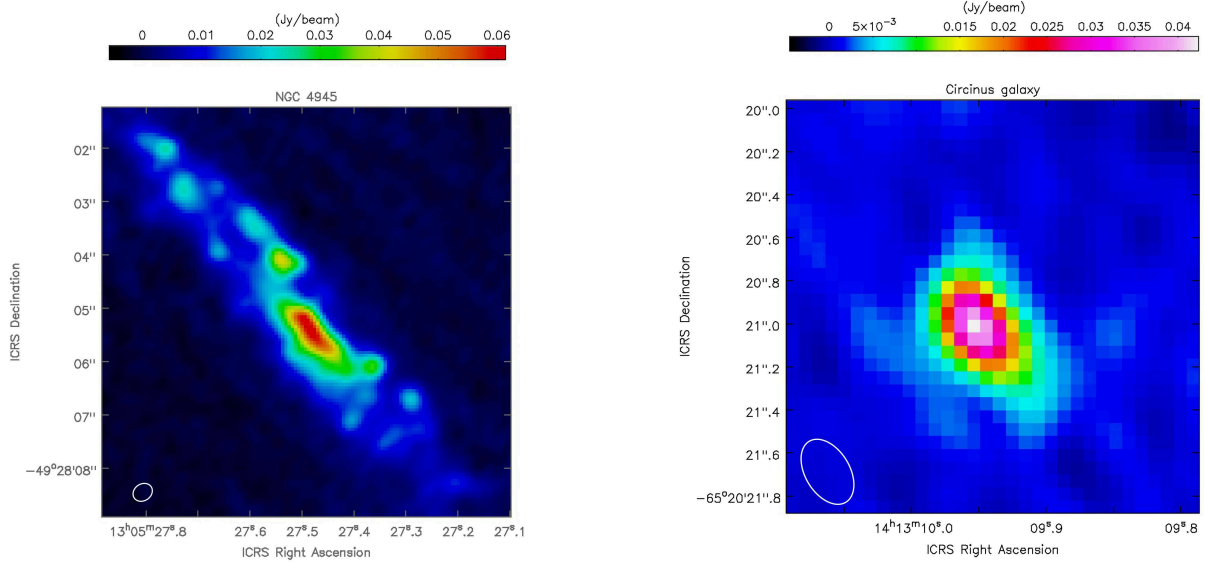


Figure 5. Continuum maps of NGC 4945 (*left*) and the Circinus galaxy (*right*) at 321 GHz (Band 7). The synthesized beams are shown in the bottom left in each panel (NGC 4945: $0.381'' \times 0.313''$; Circinus galaxy: $0.330'' \times 0.206''$). For both maps the flux densities are shown by color-scales in Jy beam^{-1} .

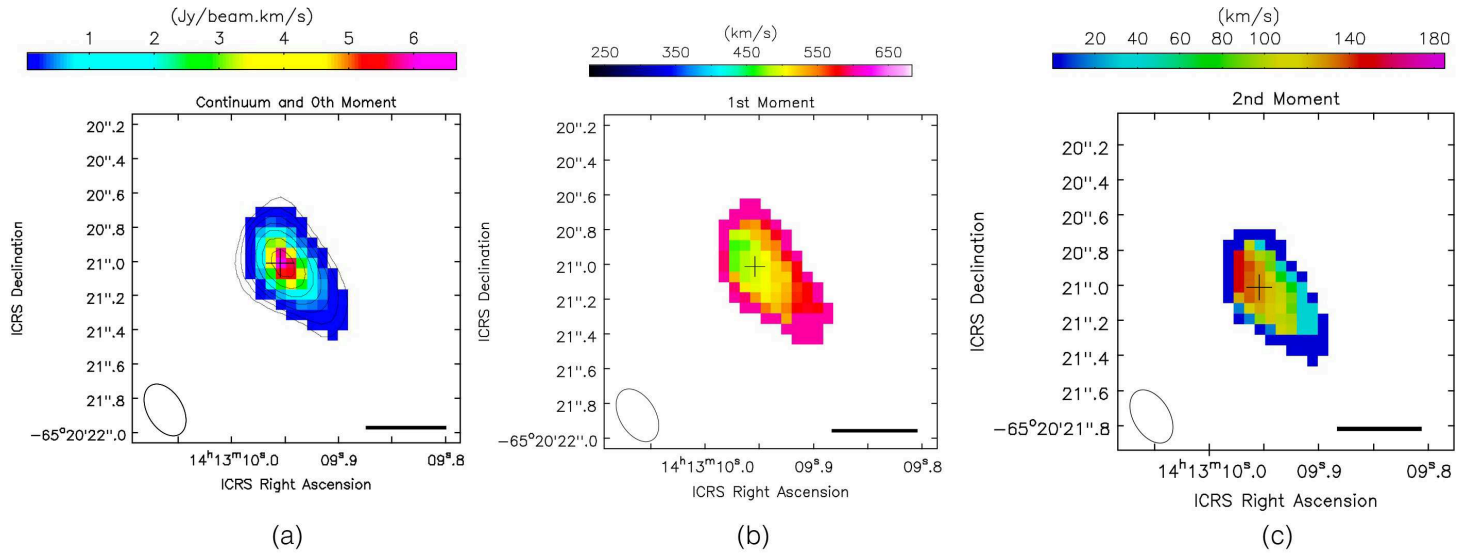


Figure 6. Color-scale maps of 321 GHz H_2O maser emission in the Circinus galaxy: (a) Integrated line intensity map (0th moment) and 321 GHz continuum with overlaying contours having a peak flux density of $42.5 \text{ mJy beam}^{-1}$ with the contour levels at 7, 9.8, 14, 19.7, 28, 39.5, and 56σ ($1 \sigma = 0.63 \text{ mJy beam}^{-1}$), (b) mean velocity (first moment) map, and (c) velocity dispersion (second moment) map. These figures are obtained from our ALMA Cycle 4 observations. The total velocity coverage of the figures is $V_{\text{LSR}} = 228\text{--}685 \text{ km s}^{-1}$. The synthesized beam sizes ($0.33'' \times 0.21''$) are shown in the bottom left of each panel. A cross in each panel marks the nucleus (the continuum peak) of the galaxy. The horizontal bar at the bottom marks 10 pc. Note that in (b) the surrounding components, reaching an extreme of $\sim 650 \text{ km s}^{-1}$ (pink) are H_2O emission extending larger than the synthesized beam size, resulting in a ring-like appearance. The blueshifted maser features peaking at $V_{\text{LSR}} \simeq 269 \text{ km s}^{-1}$ in Figure 4 (*left*) are also extended and do not show any velocity gradient on the map.

4.2.1. Origin of the maser and physical conditions giving rise to the maser

The isotropic luminosity of the 321 GHz maser emission, assuming isotropic radiation of the maser, is cal-

culated to be $\sim 65 L_{\odot}$ using the formula, $L = 1.04 \times 10^{-3} \nu D^2 \int S dv L_{\odot}$, where ν is the rest frequency (321.226 GHz), D is the distance to the Circinus galaxy of 4.2 Mpc (Freeman et al. 1977), and $\int S dv$ is the integrated intensity ($11.1 \text{ Jy km s}^{-1}$) (Humphreys et al. 2016). This value is roughly a factor of two larger than the isotropic luminosity of the 22 GHz maser emission of $\sim 32 L_{\odot}$ in the galaxy (Whiteoak et al. 1986) (adopting $D = 4.2 \text{ Mpc}$). This strongly supports the belief that the maser in the galaxy is a nuclear maser arising from AGN-activity and not from star-forming activity in the galaxy. Moreover, the position of the 321 GHz maser coincides with the radio nucleus and the significant flux variability is measured between the two epochs, which indicates that the maser may be associated with ejecta from the active nucleus such as a radio jet. Given the relatively higher maser luminosity, comparable with that of the 22 GHz megamaser known in the galaxy, we conclude that the maser amplifies the background continuum and its variability is due to the activity from a central engine in the active nucleus and so the observed 321 GHz maser in the Circinus can be categorized as a luminous H₂O megamaser.

The isotropic luminosity of the 183 GHz H₂O maser in NGC 4945, $\sim 1300 L_{\odot}$ is roughly two orders of magnitude larger than that of the 321 GHz maser in NGC 4945 at $\approx 5 L_{\odot}$ and the Circinus galaxy at $\approx 65\text{--}100 L_{\odot}$ (this paper; Humphreys et al. 2016; Hagiwara et al. 2016; Pesce et al. 2016). The upper state energies (E_u/k) of the H₂O emission for the 22 GHz and 183 GHz transition are 644 K and 205 K, respectively, while E_u/k for the 321 GHz transition is much higher: 1862 K. In NGC 4945, the energy of a significant portion of dense gas giving rise to maser amplification may not be sufficiently high enough for intense 321 GHz maser to arise, while it could be sufficient for elevating the strong 183 GHz maser emission. Therefore, insufficient excitation of the 321 GHz maser in NGC 4945 could make the strength of the maser weaker than that of the 183 and 22 GHz masers (Humphreys et al. 2016). It is therefore most likely that the strength of the 183 GHz maser in the Circinus galaxy will be greater than the 321 GHz maser in the galaxy in future observations. However, due to the higher excitation condition required for the 321 GHz maser, it is more likely that the 321 GHz masers can probe regions closer to the nucleus, which can be verified with higher angular resolution observations.

4.2.2. Velocity Gradient

One of the most exciting results from our observations is that part of the velocity field of the dense molecular gas within $\sim 6 \text{ pc}$ of the nucleus in the Circinus

galaxy has been resolved at our $\sim 0.3''$ spatial resolution. As is evident in Figure 6(b), there is a distinct velocity gradient in the 321 GHz H₂O maser emission spanning $\sim 110 \text{ km s}^{-1}$ in the first moment map. Figure 6(c) shows the second moment map which, as for Figure 6(b), is produced from the spectral-line cube containing maser features lying at $V_{\text{LSR}} = 256\text{--}670 \text{ km s}^{-1}$. This indicates that the maser emission is partly resolved in our second epoch observation at $\sim 0.3''$ ($\sim 6 \text{ pc}$) resolution, although neither velocity gradient nor velocity dispersion was found in the first epoch observation in 2011 (Hagiwara et al. 2013). This is likely to have arisen from the improvement in (u, v) coverage due to the significantly larger number of baselines, as a result of the number of antennas increasing from 18 to 47, and the longer integration time of 28 minutes, compared to 18 minutes in the first epoch.

Assuming that the observed masers are on a simple circular disk with a rotational velocity of V_{rot} at a radius r from the nucleus, the observed velocity gradient (dV/dl) along $\text{PA} = 35^\circ$ can be expressed as $dV/dl \simeq d(V_{\text{rot}} \sin\theta \sin i)/d(r\theta) \simeq V_{\text{rot}} \sin i/r$, where $l(=r\theta)$ is the projected distance, i is the disk inclination, and the approximation of $\sin\theta \simeq \theta$ is being made. Adopting the disk inclination of $>75^\circ$ ($\sin i \simeq 1$) estimated from the near-infrared emission (Tristram et al. 2014) or the CO disk with $r = 100\text{--}600 \text{ pc}$ (Curran et al. 2008), together with the observed parameters of $dV/dl = 8.8 \text{ km s}^{-1} \text{ pc}^{-1}$ and $V_{\text{red}} - V_{\text{sys}} = 682 \text{ km s}^{-1} - 433 \text{ km s}^{-1} = V_{\text{rot}} \simeq 250 \text{ km s}^{-1}$, r is estimated to be $\sim 28 \text{ pc}$. Since the most red- or blue-shifted features are interpreted as originating in an edge-on disk (e.g., Miyoshi et al. 1995), the rotation speed ranges up to $\sim 250 \text{ km s}^{-1}$ using the most Doppler-shifted velocity of $V_{\text{LSR}} \simeq 682 \text{ km s}^{-1}$. This value is to the “lower” rotation velocity ($\sim 260 \text{ km s}^{-1}$) of the sub-parsec scale disk in the Circinus galaxy, estimated from the 22 GHz maser emission (McCallum et al. 2009), compared to the Keplerian rotation velocity ($\sim 1100 \text{ km s}^{-1}$) of the disk in NGC 4258. Considering a simple circular motion around the nucleus, we estimate the dynamical mass (M_{dyn}) confined within the central 28 pc to be $\sim 4.3 \times 10^8 M_{\odot}$, which is approximately two orders of magnitude larger than the enclosed mass of $\sim 1.7 \times 10^6 M_{\odot}$ within $r = 0.1 \text{ pc}$ that was measured by VLBI observations, assuming a circular motion (Greenhill et al. 2003b).

We note that the derived value of the dynamical mass ($r \lesssim 28 \text{ pc}$) is comparable with that of the larger scale dynamical mass of $\sim 3.2 \times 10^8 M_{\odot}$ within the central 140 pc (Curran et al. 1998) and approximately two orders of magnitude larger than the total molecular mass of $M_{\text{H}_2} \approx 3 \times 10^6 M_{\odot}$ within the central $\sim 75 \text{ pc}$ in

the circumnuclear disk probed by CO (3–2) molecular gas with the deconvolved source size of $3.62'' \times 1.66''$ ($\sim 76 \text{ pc} \times 35 \text{ pc}$) (Izumi et al. 2018). This gives a gas mass fraction of only $M_{\text{H}_2}/M_{\text{dyn}} \approx 0.6\%$ within the central 28 pc.

For the Circinus galaxy, a molecular gas fraction in the central 500 pc of $M_{\text{H}_2}/M_{\text{dyn}} \approx 50\%$ has been reported (Curran et al. 2008). It is suggested that the fraction of the gas mass is up to 25% of the dynamical mass in spiral galaxies (Young and Scoville 1982).

This discrepancy is probably caused by our assumption that the 321 GHz maser traces the outer part of the central disk within the central $\sim 28 \text{ pc}$, which would result in an overestimate of the dynamical mass on a scale of 10 pc.

If the 321 GHz maser resides in the 22 GHz maser disk with $r \simeq 0.1\text{--}0.4 \text{ pc}$, obtained by VLBI mapping of the 22 GHz maser (Greenhill et al. 2003b; McCallum et al. 2009), the 321 GHz masers should be located closer to the central engine than the 22 GHz masers as the 321 GHz maser requires higher temperatures than 22 GHz masers. For the 321 GHz masers, strong inversion of the emission occurs in denser regions at a gas kinetic temperature, $T_k \gtrsim 1000 \text{ K}$ and $n(\text{H}_2) = 10^8\text{--}10^{10} \text{ cm}^{-3}$. For the 22 GHz masers, the strong inversion occurs over a broader range of physical conditions, spanning T_k of $\sim 300\text{--}1000 \text{ K}$ and $n(\text{H}_2) \lesssim 10^8$ to 10^{10} cm^{-3} (Elitzur et al. 1989; Yates et al. 1997).

We thus postulate that the 321 GHz maser traces the inner part of the masing disk with $r = 0.1\text{--}0.4 \text{ pc}$, as in the circumnuclear disk illuminated by X-rays the temperature increases closer to the central engine (e.g., Neufeld & Maloney 1995). Alternatively, the observed H_2O velocity gradient could trace non-circular motions and may not be connected to the overall velocity field on that scale.

Since the position angle of the detected gradient is comparable to that of the synthesized beam (see Table 3), the intrinsic position angle of the velocity gradient is unknown. However, the position angle ($35^\circ \pm 1^\circ$) of the maser emission deconvolved by the synthesized beam largely agrees with that of the 22 GHz H_2O maser disk ($29^\circ \pm 3^\circ$ at $r = 0.1 \text{ pc}$, and $56^\circ \pm 6^\circ$ at $r = 0.4 \text{ pc}$) (Greenhill et al. 2003b). This suggests that the inner part of each gas structure has similar position angles on all spatial scales (Curran et al. 2008).

Further observations at higher angular resolution would enable us to clarify the inner part of gaseous structure and the true origin of the velocity gradient.

4.2.3. 22 GHz Maser and 321 GHz Maser Comparison

The VLBI study of the 22 GHz maser emission by Greenhill et al. (2003b) revealed the spatial distribution of the individual maser features within the total extent of $\sim 0.04'' \times 0.09''$ ($\sim 0.8 \times 1.9 \text{ pc}$) and the origins of those maser sources were divided into two categories: the thin disk or outflows in the galaxy. They found that the velocity range of the maser emission associated with outflows is up to $\sim \pm 160 \text{ km s}^{-1}$ from the systemic velocity, which corresponds to $V_{\text{LSR}} \simeq 300\text{--}570 \text{ km s}^{-1}$, while the disk maser emission spans $V_{\text{LSR}} \simeq 250\text{--}280 \text{ km s}^{-1}$ in the blueshifted velocity range and $V_{\text{LSR}} \simeq 570\text{--}700 \text{ km s}^{-1}$ in the redshifted range. The bulk of the emission in the 321 GHz maser spectra has been detected in blue- and red-ward velocities but not at $V_{\text{LSR}} \simeq 300\text{--}500 \text{ km s}^{-1}$, which implies that the 321 GHz maser features in the blue- and redshifted velocity ranges largely originate from the thin disk, as in the case of the 22 GHz masers revealed by the VLBI study. However, in the case of the 321 GHz maser, it is not possible to distinguish whether the maser originates from a disk, an outflow, or both a disk and outflow due to lack of spatial resolution of our ALMA observations.

Contrary to the disk maser, on 2017 May 6 (Figure 2 and Figure 4(left)), strong features centered on $V_{\text{LSR}} = 359.29 \text{ km s}^{-1}$ appeared in the 321 GHz spectrum, while blueshifted features centered around $V_{\text{LSR}} = 380 \text{ km s}^{-1}$ were found in the 22 GHz maser spectrum. We interpret this to mean that these blueshifted features, that appeared at both 321 GHz and 22 GHz, are outflow masers that flared at the same period and they are associated with significant shocks with the surrounding molecular materials in the nuclear region. This also supports the hypothesis that the 321 GHz and 22 GHz masers are powered by the central engine, as argued in Section 4.1.

It should be noted that submillimeter stellar H_2O masers are often found to be associated with outflow jets, while the 22 GHz masers are primarily found in disks (e.g., Patel et al. 2007). However, it still remains unclear to what extent these findings can be applied to the cases of extragalactic 321 GHz H_2O masers.

4.2.4. Velocity Dispersion

In Figure 6(c), we find a high velocity dispersion region, with a velocity dispersion (σ_v) of $\sim 148 \text{ km s}^{-1}$, where the rotation velocity ($V_{\text{rot}} = V_{\text{LSR}} - V_{\text{SYS}}$) is 29 km s^{-1} in the first moment map, is offset to the northeast of the continuum nucleus and a gradient of the velocity dispersion is seen between $V_{\text{LSR}} \simeq 98 \text{ km s}^{-1}$ and 148 km s^{-1} along the southwest to northeast direction. We speculate that velocities at the northeastern part are more blueshifted than those at the southeast part in the

first moment map, which reduces the opacity and results in making the turbulent molecular gas appear stronger (Imanishi et al. 2018, 2020). It is interesting to note that the relative velocity dispersion values of V_{rot}/σ_v (Treister et al. 2020) increase from ~ 0.2 to 1.4 from the northeast to the southwest direction and the velocity dispersion distribution is similar to the velocity gradient. It is not certain whether the velocity dispersion distribution can be explained by our simple speculation, however it could be dynamically linked to circular or non-circular motion on scales of 10 pc.

Future sub-millimeter VLBI mapping of the 321 GHz H₂O masers at milliarcsecond resolution (e.g., Fish et al. 2013) should be able to clarify the sub-parsec-scale kinematics of the galaxy by pin-pointing the distributions of each of the maser features.

5. CONCLUSIONS

We have observed H₂O masers in the 321 GHz transition toward the nearby active galactic nuclei NGC 4945 and the Circinus galaxy at $\sim 0.3''$ angular resolution with ALMA Band 7. Comparison of two epochs of ALMA observations show that the flux densities of the 321 GHz H₂O masers in the galaxies are significantly variable on timescales of 4–5 years and the nuclear continuum emission varies in a correlated fashion with the maser in NGC 4945, while the correlation between the maser and the nuclear continuum is less certain in the Circinus galaxy. The significant variability in the flux densities has confirmed that the observed H₂O emission arises from nuclear masers. With the 70 m telescope at Tidbinbilla we also conducted single-dish measurements of the 22 GHz maser emission over 3–5 epochs between the two ALMA observations toward the galaxies to compare the variability of the fluxes and velocities between the 321 GHz and 22 GHz maser lines. This revealed in the Circinus galaxy the flaring features of the 321 GHz and 22 GHz maser emission were found largely in the same blueshifted velocity range on the same day. It is thus likely that the 321 GHz and 22 GHz masers originate in similar kinematics and physical conditions.

Contrary to the previous lower spatial resolution observations, made with a much smaller number of antennas, in the Circinus galaxy we detected a velocity gradient and dispersion, traced by the 321 GHz H₂O maser emission, in a roughly southwest to northeast direction. This position angle is similar to that of the sub-parsec scale thin disk probed by the 22 GHz H₂O masers. With the velocity gradient spanning $\sim 110 \text{ km s}^{-1}$, we estimate the dynamical mass within the central 28 pc to be $\sim 4.3 \times 10^8 M_{\odot}$, which is significantly larger than the dynamical mass and the molecular gas mass within the

similar radii. Therefore, the observed velocity gradient does not likely trace the extension of the sub-parsec-scale 22 GHz maser disk but might indicate non-circular motion rather than the simple circular motion of the disk on that scale. If the 321 GHz maser is in the circumnuclear disk, it should be observed closer to the central engine than the 22 GHz masers as the excitation of 321 GHz maser needs a higher temperature in denser gas.

We speculate that blueshifted H₂O maser emission at north-eastern region reduces the opacity, making turbulence of molecular gas more conspicuous, which results in the higher velocity dispersion at that region. The gradient of the velocity dispersion is also found along the same position angle as the velocity gradient. Its origin is uncertain from our data, however it could be physically connected to organized movements like circular motion. Overall, the comparison of our data to the earlier VLBI studies of the 22 GHz H₂O maser suggests that the 321 GHz H₂O maser could not trace an extension of the sub-parsec scale thin disk but the variable blue-shifted features might trace the nuclear outflows. Higher spatial observations using ALMA or future sub-millimeter VLBI might reveal whether the 321 GHz H₂O maser probes a dynamical structure of inner parsecs or inner part of the circumnuclear disk in the Circinus galaxy.

We thank the anonymous referee for useful comments. YH thanks Kazuya Saigo for his support with the ALMA data reduction pipeline. This work was supported by JSPS KAKENHI Grant Number JP15H03644 (YH) and 21K03632 (MI). This paper makes use of the following ALMA data: ADS/JAO.ALMA #2016.1.00150.S, #2011.0.00121.S. ALMA is a partnership of ESO, NSF and NINS, together with NRC, MOST and ASIAA, and KASI, in cooperation with the Republic of Chile. The Joint ALMA Observatory is operated by ESO, AUI/NRAO and NAOJ. The Tidbinbilla 70-m telescope, DSS-43, is part of the NASA Deep Space Network and is operated by CSIRO. This research has made use of the NASA/IPAC Extragalactic Database (NED), which is funded by the National Aeronautics and Space Administration and operated by the California Institute of Technology. This project made use of the Smithsonian Astrophysical Observatory 4×32k-channel spectrometer (SAO32k) and the TAMS observatory Ctrl observing system, which were developed by L. Greenhill (Center for Astrophysics), I. Zaw (New York University Abu Dhabi), D. Price, and D. Shaff, with funding from SAO and the NYUAD Research Enhancement Fund and in-kind support from the Xilinx University Program.

Facilities: ALMA, Tidbinbilla 70m (DSS-43)

Software: CASA, AIPS, ASAP, GBTIDL

REFERENCES

- Arévalo, P., Bauer, F. E., Puccetti, S., et al. 2014, *ApJ*, 791, 81
- Braatz, J. A., Wilson, A. S., & Henkel, C. 1994, *ApJL*, 437, L99
- Braatz J. A., Wilson A. S., & Henkel C. 1996, *ApJS*, 106, 51
- Braatz, J. A., Wilson, A. S., Henkel, C., Gough, R., & Sinclair, M. 2003, *ApJS*, 146, 249
- Braatz, J. A., & Gugliucci, N. E. 2008, *ApJ*, 678, 96
- Cernicharo, J., Pardo, J. R., & Weiss, A. 2006, *ApJ*, 646, L49
- Curran, S. J., Johansson, L. E. B., Rydbeck, G., & Booth, R. S. 1998, *A&A*, 338, 863
- Curran, S. J., Rydbeck, G., Johansson, L. E. B., & Booth, R. S. 1999, *A&A*, 344, 767
- Curran, S. J., Koribalski, B. S., & Bains, I. 2008, *MNRAS*, 389, 63
- de Vaucouleurs, G., de Vaucouleurs, A., Corwin, H. G., et al. 1991, *Third Reference Catalog of Bright Galaxies* (Berlin: Springer)
- Dos Santos, P. M., & Lépine, J. R. D. 1979, *Nature*, 278, 34
- Elitzur, M., Hollenbach, D. J., & McKee, C. F. 1989, *ApJ*, 346, 983
- Fish, V., Alef, W., Anderson, J., et al. 2013, *arXiv:1309.3519*
- Freeman, K. C., Karlsson, B., Lynga, G., et al. 1977, *A&A*, 55, 445
- Galametz, M., Zhang, Z.-Y., Immer, K., et al. 2016, *MNRAS*, 462, L36
- Greenhill, L. J., Ellingsen, S. P., Norris, R. P., et al. 1997a, *ApJ*, 474, L103
- Greenhill, L. J., Moran, J. M., & Herrnstein, J. R. 1997b, *ApJ*, 481, L23
- Greenhill, L. J., Kondratko, P. T., Lovell, J. E. J., et al. 2003a, *ApJL*, 582, L11
- Greenhill, L. J., Booth, R. S., Ellingsen, S. P., et al. 2003b, *ApJ*, 590, 162
- Greenhill, L. J., Kondratko, P. T., Moran, J. M., et al. 2009, *ApJ*, 707, 787
- Hagiwara, Y., Diamond, P. J., & Miyoshi, M. 2002, *A&A*, 383, 65
- Hagiwara, Y., Diamond, P. J., Miyoshi, M., et al. 2003, *MNRAS*, 344, L53
- Hagiwara, Y., Miyoshi, M., Doi, A., & Horiuchi, S. 2013, *ApJL*, 768, L38
- Hagiwara, Y., Horiuchi, S., Doi, A., Miyoshi, M., & Edwards, P. G. 2016, *ApJ*, 827, 69
- Hagiwara, Y., Doi, A., Hachisuka, K., & Horiuchi, S. 2018, *PASJ*, 70, 54
- Henkel, C., Peck, A. B., Tarchi, A., et al. 2005, *A&A*, 436, 75
- Humphreys, E. M. L., Greenhill, L. J., Reid, M. J., et al. 2005, *ApJ*, 634, L133
- Humphreys, E. M. L., Vlemmings, W. H. T., Impellizzeri, C. M. V., et al. 2016, *A&A*, 592, L13
- Imanishi, M., Nakanishi, K., Izumi, T., et al. 2018, *ApJL*, 853, L25
- Imanishi, M., Nguyen, D. D., Wada, K., et al. 2020, *ApJ*, 902, 99
- Imanishi, M., Hagiwara, Y., Horiuchi, S., et al. 2021, *MNRAS*, 502, L79
- Isobe, N., Kubota, A., Makishima, K., et al. 2008, *PASJ*, 60, 241
- Iwasawa, K., Koyama, K., Awaki, H., et al. 1993, *ApJ*, 409, 155
- Izumi, T., Wada, K., Fukushige, R., Hamamura, S., & Kohno, K. 2018, *ApJ*, 867, 48
- Kondratko, P. T., Greenhill, L. J., Moran, J. M., et al. 2006, *ApJ*, 638, 100
- König, S., Martín, S., Muller, S., et al. 2017, *A&A*, 602, A42
- Kuiper, T. B. H., Franco, M., Smith, S., et al. 2019, *Journal of Astronomical Instrumentation*, 8, 1950014
- Madejski, G., Życki, P., Done, C., et al. 2000, *ApJL*, 535, L87
- Maloney, P. R. 2002, *PASA*, 19, 401
- Marconi. A., Moorwood, A. F. M., Origlia, L., & Olivia, E. 1994, *Messenger*, 78, 20
- Marinucci, A., Bianchi, S., Fabbiano, G., et al. 2017, *MNRAS*, 470, 4039
- McCallum, J. N., Ellingsen, S. P., Jauncey, D. L., Lovell, J. E. J., & Greenhill, L. J. 2005, *AJ*, 129, 1231
- McCallum, J. N., Ellingsen, S. P., Lovell, J. E. J., Phillips, C. J., & Reynolds, J. E. 2009, *MNRAS*, 392, 1339
- McMullin, J. P., Waters, B., Schiebel, D., et al. 2007, *Astronomical Data Analysis Software and Systems XVI*, 376, 127
- Miyoshi, M., Moran, J., Herrnstein, J., et al. 1995, *Nature*, 373, 127
- Nakai, N., Inoue, M., Miyazawa, K., Miyoshi, M., & Hall, P. 1995, *PASJ*, 47, 771
- Neufeld, D. A., Maloney, P. R., & Conger, S. 1994, *ApJL*, 436, L127
- Neufeld, D. A. & Maloney, P. R. 1995, *ApJL*, 447, L17

- Patel, N. A., Curiel, S., Zhang, Q., et al. 2007, *ApJL*, 658, L55
- Pesce, D. W., Braatz, J. A., & Impellizzeri, C. M. V. 2016, *ApJ*, 827, 68
- Puccetti, S., Comastri, A., Fiore, F., et al. 2014, *ApJ*, 793, 26
- Tarchi, A., Castangia, P., Columbano, A., et al. 2011, *A&A*, 532, A125
- Treister, E., Messias, H., Privon, G. C., et al. 2020, *ApJ*, 890, 149. doi:10.3847/1538-4357/ab6b28
- Tristram, K. R. W., Burtscher, L., Jaffe, W., et al. 2014, *A&A*, 563, A82
- Tully, R. B., Courtois, H. M., Dolphin, A. E. et al. 2013, *AJ*, 146, 86
- van Moorsel, G., Kembell, A., & Greisen, E. 1996, *Astronomical Data Analysis Software and Systems V*, 101, 37
- Whiteoak, J. B., & Gardner, F. F. 1986, *MNRAS*, 222, 513
- Yang, Y., Wilson, A. S., Matt, G., et al. 2009, *ApJ*, 691, 131
- Yates, J. A., Field, D., & Gray, M. D. 1997, *MNRAS*, 285, 303
- Young, J. S., & Scoville, N. 1982, *ApJ*, 258, 467
- Zhang, J. S., Henkel, C., Kadler, M., et al. 2006, *A&A*, 450, 933